DNA-guided lattice remodeling of carbon nanotubes

Zhiwei Lin[1,*], **Leti Beltran**[2], **Zeus A. De los Santos**[1], **Yinong Li**[3], **Tehseen Adel**[4], **Jeffrey A Fagan**[1], **Angela R. Hight Walker**[4], **Edward H. Egelman**[2], **Ming Zheng**[1,*]

[1]Materials Science and Engineering Division, National Institute of Standards and Technology, Gaithersburg, MD 20899, USA

[2]Department of Biochemistry and Molecular Genetics, University of Virginia, Charlottesville, VA 22908, USA

[3]South China Advanced Institute for Soft Matter Science and Technology, School of Emergent Soft Matter, South China University of Technology, Guangzhou 510640, China

[4]Quantum Metrology Division, National Institute of Standards and Technology, Gaithersburg, MD 20899, USA

Abstract

Covalent modification of carbon nanotubes is a promising strategy to engineer their electronic structures. However, keeping modification sites in registration with a nanotube lattice is challenging. We report here a solution using DNA-directed, guanine (G)-specific crosslinking chemistry. By DNA screening we identify a sequence $C_3GC_7GC_3$ whose reaction with an (8,3) enantiomer yields minimum disorder-induced Raman mode intensities and photoluminescence Stokes shift, suggesting ordered defect array formation. Single-particle cryo-EM shows that the $C_3GC_7GC_3$ functionalized (8,3) has an ordered helical structure with a 6.5Å periodicity. Reaction mechanism analysis suggests that the helical periodicity arises from an array of G-modified carbon-carbon bonds separated by a fixed distance along an armchair helical line. Our findings may be used to remodel nanotube lattices for novel electronic properties.

One-Sentence Summary:

A DNA-guided synthetic pathway leading to lattice remodeling of carbon nanotubes is discovered.

Keywords

supramolecular chemistry; organic quantum material; carbon nanotube; DNA; cryo-EM

Synthesis of carbon-based quantum materials can in principle employ rich organic chemistry to realize novel properties via atomic-precision structural engineering. Over 50 years ago,

W. A. Little proposed a room-temperature organic superconductor model composed of a one-dimensional conducting chain with an array of polarizable side chains attached (1). In the ensuing years, numerous efforts had been made but failed to verify Little's proposal (2). In 2016, the mechanism underlying Little's model –electron attraction mediated by polarizable groups– was confirmed for the first time (3). The study used a single-wall carbon nanotube (SWCNT) as the one-dimensional conducting chain, along which a nanotube circuitry was constructed to provide a single polarizable "side chain". This work suggests a route to the Little model by chemically implanting polarizable groups in registration with a SWCNT lattice, but the task is deemed formidable (4). A major challenge is to control reaction sites along the nanotube, which seems insurmountable because half population of carbon atoms on a SWCNT are chemically equivalent and are enantiomers of the remaining half. Here we report a DNA-guided chemical reaction to overcome the challenge. We screen reaction products by resonance Raman and photoluminescence (PL) spectroscopy, and inspect the structures of promising candidates by single-particle cryo-EM. Our findings demonstrate feasibility to create a wide range of SWCNT derivatives in general, and to build a Little model in particular.

Broadly speaking, covalent modification of SWCNTs is a promising route towards organic quantum materials (5–7). With all atoms on their surfaces, SWCNTs are more amenable than other solid-state materials to precision molecular engineering by wet chemistry. In addition, various chiral forms of SWCNTs made available by sorting (8) offer a diverse range of electronic structures for further chemical tailoring. Recently, Weisman *et al.* reported a photochemical reaction of DNA-wrapped SWCNTs with singlet oxygen that covalently links guanine (G) to the side wall of SWCNTs (6). Even though the chemical nature of the covalent link was not fully revealed, and the structure of the reaction product rather disordered (9), we are nevertheless inspired to pursue ordered SWCNT lattice modification with the idea of finding more effective ways to explore the nanotube chirality and DNA sequence space.

To speed up sequence screening and to promote ordered structure formation, we have explored conditions for the guanine functionalization reaction of SWCNTs. We find that the previously reported aqueous phase photochemical reaction of Rose Bengal (RB) mediated guanine crosslinking with SWCNTs (6) also works in methanol/water mixed solvents. In 50 % v/v methanol, the reaction proceeds slower than that in water (reaction time 60 min *versus* 15 min in water); consumption of RB sensitizer is decreased dramatically; and RB binding to SWCNTs, which may adversely affect DNA wrapping structure and crosslinking site, is also minimized. All these changes should favor homogeneous product formation. Combining this new reaction condition with a previously established process (10) for DNA/surfactant exchange, we have devised a one-pot chemistry (Fig. 1A, Figs. S1–5) that can efficiently react any G-containing sequence with any single-chirality SWCNT species [*e.g.*, (6,5), (9,1), (8,3), *etc.*.] purified independently via various techniques (8). Excess DNA is present during the reaction in order to refill exposed nanotube surfaces arising from reaction-induced DNA structure contraction, eliminating a potential source of inhomogeneous functionalization.

We have employed spectroscopic tools to monitor the reaction (Fig. 1, Figs. S6–7). Figs. 1B–D present a data set from a reaction on an (8,3) enantiomer (normalized circular dichroism signal at the $E_{22} = -42$ mdeg, which according to theoretical analysis corresponds to a right-handed enantiomer(11)). Hereafter we denote the enantiomer simply as (8,3) unless indicated otherwise. Figs. 1B and 1C show, respectively, the expected red-shift of the E_{11} absorption and PL peak after functionalization. Fig. 1D shows resonance Raman spectra of unfunctionalized (black trace) and functionalized (8,3) (red trace). In addition to the well-documented D peak, we find another disorder-induced peak: the intermediate frequency mode (IFM)(12, 13) at 387 cm^{-1}, its overtone 2 IFM at 775 cm^{-1}, and its combination modes with D: D ± IFM at 905 and 1680 cm^{-1}, respectively. There is a dramatic intensity enhancement of the D and IFM modes in functionalized tubes. In contrast, 2IFM and D ± IFM peaks remain weak and unchanged after functionalization, consistent with their origin from two-phonon, second-order scattering processes (12).

To gain insight into the reaction mechanism, we have functionalized (8,3) using a set of DNA sequences with varying G content. With increasing G content, the functionalized (8,3) shows a gradual increase in both D and IFM peak intensity (Figs. 2A and 2B), and more red-shifted and broadened PL and absorbance peaks (Figs. 2C and 2D). These observations are consistent with the previous study using mixed chirality tubes (6). However, using chirality-pure SWCNTs allows us to determine unambiguously the absorption and PL peak positions of the functionalized tube, and calculate its absorption peak shift and Stokes shift *SS, i.e.*, the energy difference between the absorption and PL peak, as a function of G content or defect density. The absorption peak shift increases with G content (Fig. 2E), but its amplitude is less than 27 meV, about 10 times smaller than that typically observed for an sp^3 defect (14). This difference is striking considering that the defect density ($\approx 10^0$/nm) in guanine modified tubes (15) is about two orders of magnitude higher than that in sp^3 modified tubes (5). The *SS* also increases with defect density (Fig. 2E) – a trend opposite to that observed for sp^3 defect (14). In addition, we find a quantitative relationship between *SS* and full width at half maximum (FWHM = W) of the PL peaks, suggesting that modified and unmodified carbon atoms are isovalent as reasoned below. In Fig. 2F, we plot *SS vs* W^2 and fit the data well ($R^2 = 0.98$) with $T = 349.3$K using eq. (1), where k is the Boltzmann constant and T is the effective exciton temperature equal to or above the ambient temperature.

$$SS = \frac{W^2}{8 \ln 2 \, kT} \cong 0.18 \frac{W^2}{kT} \tag{1}$$

Eq. (1) has been used to describe excitons in 2D quantum wells and 3D alloy semiconductors where disordered isovalent substitution creates shallow traps (16, 17). It attributes the observed *SS* to the thermalization of excitons in an inhomogeneously broadened band. Combining all of these spectroscopic observations, we exclude sp^3 defect formation by guanine functionalization and conclude that the chemistry creates a modified sp^2 defect that is isovalent to the original sp^2 carbon in the pristine SWCNT.

To differentiate two types of disorder originating from the defect density itself and defect distribution pattern, we have designed a set of 15-mer G/C sequences containing two Gs

separated by a varying number of Cs (Fig. 3A) for the (8,3) functionalization chemistry. We find that disorder-induced D and IFM peak intensities change as a function of the inter-G spacing, reaching a surprisingly deep minimum when the spacing is 7 (Figs. 3B and 3C). The *SS* and PL peak linewidth also show minimum values at that spacing (Figs. 3D and 3E). These observations appear to be dependent on nanotube chirality, since left- and right-handed (6,5)s functionalized by the same set of sequences yield different spectral patterns (Fig. S7).

We offer a qualitative analysis of the data shown in Fig. 3. According to the mechanism of defect-induced Raman modes (12, 18), the observed peak intensity is proportional to the extent of elastic electron scattering by defects. For sequences used in our study, we estimate that a SWCNT contains 1–5 guanine modified sites per nm tube length based on molecular dynamics simulations of a typical DNA wrapping structure on a SWCNT (15). Because the size of excitons is 2 to 3 nm (19), electron scattering is expected to involve multiple defect sites, and is sensitive to not only the defect density but also the degree of order of the defect array. The minimum D and IFM peak intensities shown in Fig. 3 are thus interpreted as resulting from an ordered defect array generated by the 2G-7 sequence. This conclusion is also consistent with the observed minimum *SS* for the same sequence, as *SS* is another measure of disorder for semiconductors with isovalent substitution (16, 17).

To independently evaluate the spectroscopy-derived result, we have applied single-particle cryo-EM to measure 2G-7-(8,3) hybrid structure before and after functionalization. Cryo-EM imaging of 2G-7 functionalized (8,3) reveals filaments of approximately 20Å in diameter (Fig. S11). In the non-functionalized structure coated with 2G-7, an averaged power spectrum from $\approx 2\times10^5$ images of particle segments yields no detectable features (Fig. S12), implying a disordered DNA wrapping structure. In the functionalized structure, we have detected a layer line pattern characteristic of a 1-start helix with 6.5 Å helical pitch visible from the averaged power spectrum of selected segments (Fig. 4A). The helical structure is also visible in the two-dimensional (2D) class average (Fig. 4B). *Ab initio* reconstruction, an unbiased and reference free approach, was employed to generate a 3D reconstruction of the DNA coated nanotube (Fig. 4C). Fig. 4D shows a highly averaged version of that reconstruction, with an atomic model for the SWCNT. Due to the low signal-to-noise ratio in these cryo-EM images, and the apparent lack of any other periodicities present, we have imposed a helical averaging of the density along the 6.5 Å pitch helix. The unfiltered 3D map (Fig. 4C) shows a coherence length that is about 10 nm long, shorter than the full length of the segments used. The density in Figs. 4C and 4D is shown as a left-handed helix, however, true handedness was not determined.

The 6.5 Å periodicity observed by cryo-EM provides support for the model of ordered defect array formation and an important clue to the mechanism of guanine functionalization. As discussed earlier, a correct reaction mechanism should yield a modified carbon that largely maintains its sp^2 character. Indeed, such chemistry has been well-documented (20, 21) and forms the basis for our proposal shown in Figs. 4E, 4F, and S14B. Guanine oxidation by singlet oxygen has a plethora of pathways and products depending on reaction conditions and structural context, but a common initial step is oxidation of the C_8 carbon on the imidazole ring (22). We propose that the C_8 carbon becomes electrophilic upon

oxidation, and then undergoes a 2+1 cycloaddition with a nearby C-C bond on a SWCNT to yield a three-membered ring. This is followed by the C-C bond cleavage and concomitant ring opening due to ring strain, leaving C_8 to bridge the two carbons from the SWCNT and restore their sp^2 character. Theoretical calculation (20) predicts that this type of reaction is most favorable on C-C bonds with large curvature or bond strain, consistent with a previous observation from the guanine functionalization chemistry (Figure 2C in reference (6)). In (8,3), there are three types of C-C bonds with distinct curvatures. C-C bonds along a helical armchair line shown in Fig. 4E possess the largest curvature. We note that the pitch p of this helical line is an intrinsic length scale of (8,3) determined solely by its chiral index *(n, m)* and C-C bond length a_c: $p = a_c\sqrt{n^2 + m^2 + nm}\frac{n-m}{n+m} = 6.45\ \mathring{A}\ \left(for\ a_c = 1.44\ \mathring{A}\right)$, matching that observed by the cryo-EM. We therefore propose a 2G-7 wrapping structure where each of the 2Gs is covalently linked to a C-C bond along the armchair line, resulting in pinning of the DNA backbone along the same armchair line. Consistent with this functionalization-induced DNA pinning is our observation that 2G-5 and 2G-6 functionalized (8,3) also exhibit the same 6.5 Å helical pitch (Fig. S13). Manual model building for 2G-7 functionalized (8,3) followed by energy minimization yields a model shown in Fig. S14A, in which two adjacent G modification sites are separated by 5 C-C bonds along the armchair line. This equal G spacing explains minimum spectroscopy-derived structure disorder for 2G-7 functionalized (8,3).

In summary, we show that ordered SWCNT modification can be achieved by taking advantage of DNA sequence control over the spacing between adjacent reaction sites, and SWCNT's bond curvature dependent reactivity. Our finding demonstrates chemical feasibility to build a Little model. DNA-guided remodeling breaks the original symmetry of the nanotube lattice, and therefore should lead to new modes of low-energy electronic excitation. Theoretical analysis shows that helical modification of a SWCNT in registry with its lattice may induce topological electronic behavior (23, 24), suggesting that the chemistry we report here might be used to explore topological physics. We envision that future work will introduce diversity of functional groups, increase the coherent length of ordered modification, and eventually enable discovery of organic quantum materials and carbon-based metal-free catalysts (25, 26).

Supplementary Material

Refer to Web version on PubMed Central for supplementary material.

Acknowledgements

Data and materials availability:

All data needed to evaluate the conclusions in the paper are present in the paper or the Supplementary Materials.

References and Notes

1. Little WA, Possibility of Synthesizing an Organic Superconductor. Physical Review 134, A1416–A1424 (1964).

2. Jérome D, The Physics of Organic Superconductors. Science 252, 1509–1514 (1991). [PubMed: 17834876]

3. Hamo A et al. , Electron attraction mediated by Coulomb repulsion. Nature 535, 395–400 (2016). [PubMed: 27443742]

4. Kontos T, Attractive electrons from nanoengineering. Nature 535, 362–363 (2016). [PubMed: 27443737]

5. Piao Y et al. , Brightening of carbon nanotube photoluminescence through the incorporation of sp3 defects. Nature Chemistry 5, 840–845 (2013).

6. Zheng Y, Bachilo SM, Weisman RB, Controlled Patterning of Carbon Nanotube Energy Levels by Covalent DNA Functionalization. ACS Nano 13, 8222–8228 (2019). [PubMed: 31244048]

7. Yang F et al. , Chirality Pure Carbon Nanotubes: Growth, Sorting, and Characterization. Chemical Reviews 120, 2693–2758 (2020). [PubMed: 32039585]

8. Zheng M, Sorting Carbon Nanotubes. Topics in Current Chemistry 375, 13 (2017). [PubMed: 28083771]

9. Zheng Y et al. , Quantum Light Emission from Coupled Defect States in DNA-Functionalized Carbon Nanotubes. ACS Nano 15, 10406–10414 (2021). [PubMed: 34061507]

10. Streit JK, Fagan JA, Zheng M, A Low Energy Route to DNA-Wrapped Carbon Nanotubes via Replacement of Bile Salt Surfactants. Analytical Chemistry 89, 10496–10503 (2017). [PubMed: 28856894]

11. Sato N, Tatsumi Y, Saito R, Circular dichroism of single-wall carbon nanotubes. Physical Review B 95, 155436 (2017).

12. Vierck A, Gannott F, Schweiger M, Zaumseil J, Maultzsch J, ZA-derived phonons in the Raman spectra of single-walled carbon nanotubes. Carbon 117, 360–366 (2017).

13. Inaba T, Tanaka Y, Konabe S, Homma Y, Effects of Chirality and Defect Density on the Intermediate Frequency Raman Modes of Individually Suspended Single-Walled Carbon Nanotubes. The Journal of Physical Chemistry C 122, 9184–9190 (2018).

14. Berger FJ et al. , Brightening of Long, Polymer-Wrapped Carbon Nanotubes by sp3 Functionalization in Organic Solvents. ACS Nano 13, 9259–9269 (2019). [PubMed: 31381849]

15. Roxbury D, Jagota A, Mittal J, Structural Characteristics of Oligomeric DNA Strands Adsorbed onto Single-Walled Carbon Nanotubes. The Journal of Physical Chemistry B 117, 132–140 (2013). [PubMed: 23199189]

16. Gurioli M, Vinattieri A, Martinez-Pastor J, Colocci M, Exciton thermalization in quantum-well structures. Physical Review B 50, 11817–11826 (1994).

17. Felici M et al. , Compositional disorder in GaAs1-xNx:H investigated by photoluminescence. Physical Review B 74, 085203 (2006).

18. Thomsen C, Reich S, Double Resonant Raman Scattering in Graphite. Physical Review Letters 85, 5214–5217 (2000). [PubMed: 11102224]

19. Lüer L et al. , Size and mobility of excitons in (6, 5) carbon nanotubes. Nature Physics 5, 54–58 (2009).

20. Lee Y-S, Marzari N, Cycloaddition Functionalizations to Preserve or Control the Conductance of Carbon Nanotubes. Physical Review Letters 97, 116801 (2006). [PubMed: 17025914]

21. Setaro A et al. , Preserving π-conjugation in covalently functionalized carbon nanotubes for optoelectronic applications. Nature Communications 8, 14281 (2017).

22. Ye Y et al. , Formation of 13C-, 15N-, and 18O-Labeled Guanidinohydantoin from Guanosine Oxidation with Singlet Oxygen. Implications for Structure and Mechanism. Journal of the American Chemical Society 125, 13926–13927 (2003). [PubMed: 14611206]

23. Puller VI, Rotkin SV, Helicity and broken symmetry of DNA-nanotube hybrids. Europhysics Letters (EPL) 77, 27006 (2007).

24. Hu C, Michaud-Rioux V, Yao W, Guo H, Theoretical Design of Topological Heteronanotubes. Nano Letters 19, 4146–4150 (2019). [PubMed: 31117763]

25. Gong K, Du F, Xia Z, Durstock M, Dai L, Nitrogen-Doped Carbon Nanotube Arrays with High Electrocatalytic Activity for Oxygen Reduction. Science 323, 760–764 (2009). [PubMed: 19197058]

26. Liu X, Dai L, Carbon-based metal-free catalysts. Nature Reviews Materials 1, 16064 (2016).

27. Ao G, Khripin CY, Zheng M, DNA-Controlled Partition of Carbon Nanotubes in Polymer Aqueous Two-Phase Systems. Journal of the American Chemical Society 136, 10383–10392 (2014). [PubMed: 24976036]

28. Ao G, Streit JK, Fagan JA, Zheng M, Differentiating Left- and Right-Handed Carbon Nanotubes by DNA. Journal of the American Chemical Society 138, 16677–16685 (2016). [PubMed: 27936661]

29. De los Santos ZA, Lin Z, Zheng M, Optical Detection of Stereoselective Interactions with DNA-Wrapped Single-Wall Carbon Nanotubes. Journal of the American Chemical Society 143, 20628–20632 (2021). [PubMed: 34843644]

30. Lyu M, Meany B, Yang J, Li Y, Zheng M, Toward Complete Resolution of DNA/Carbon Nanotube Hybrids by Aqueous Two-Phase Systems. Journal of the American Chemical Society 141, 20177–20186 (2019). [PubMed: 31783712]
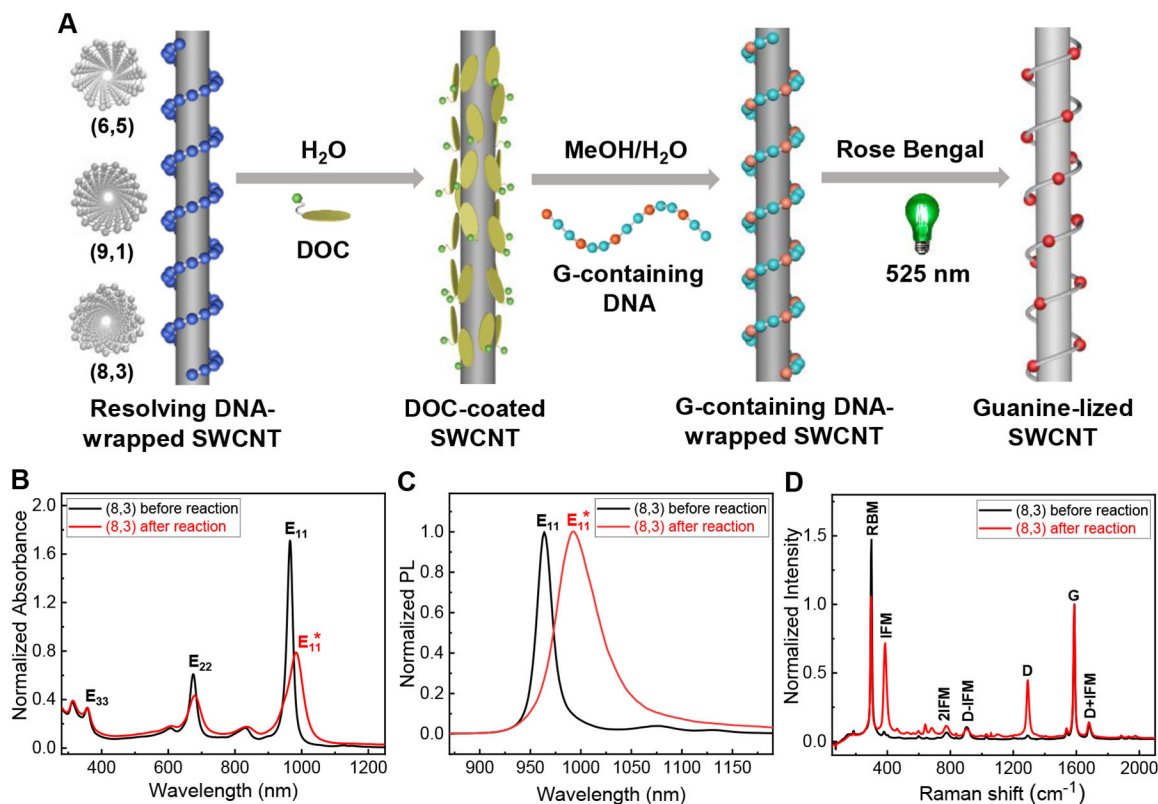
Fig. 1. One-pot photochemical reaction scheme and spectral characterization.
(A) Reaction scheme starting from resolving DNA-wrapped to guanine-functionalized (guanine-lized) SWCNT carried out in a single pot; **(B)** Absorption (normalized at E_{33}); **(C)** PL (with peak intensity normalized to 1); and **(D)** Resonance Raman spectra (normalized at the "G" peak) of (8,3) before and after reaction. Spectra in **C** and **D** are measured with 671 nm excitation corresponding to E_{22} of (8,3). The DNA sequence used in this experiment is $(GCC)_{12}$. Also see Fig. S8 for data shown in **B** and **C** before normalization.
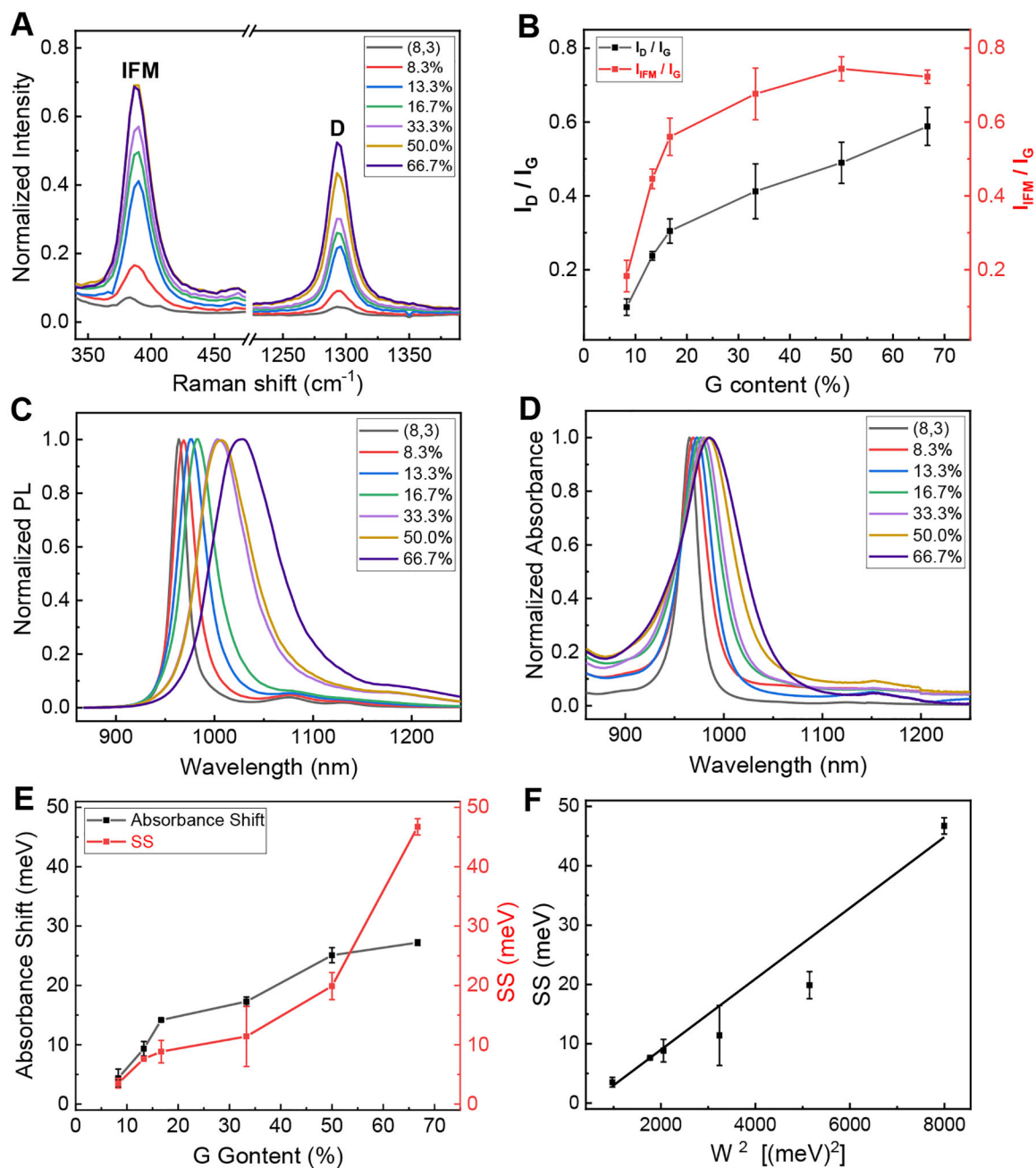
Fig. 2. Spectroscopic characterization of (8,3) functionalized with DNA of varying G content (see Table S1 for sequence information).

(**A**) and (**B**) IFM and D peak intensity (normalized by the intensity of the "G" peak) profile; (**C**) **and (D)** PL and absorbance profile; (**E**) Absorbance shift and *SS* profile; (**F**) *SS* vs W^2 and a linear fit ($R^2 = 0.98$) using eq. (1) with $T = 349.3K$. Error bar shown here and elsewhere in this work represents standard deviation derived from three independently measured values for each of three independently prepared samples. Spectra in **A**, **C** and **D** are measured with 671 nm excitation. Also see Fig. S9 for original data.

A

2G-0: CCCCCCC**GG**CCCCCC

2G-1: CCCCCC**G**C**G**CCCCCC

2G-3: CCCCC**G**CCC**G**CCCCC

2G-5: CCCC**G**CCCCC**G**CCCC

2G-6: CCCC**G**CCCCCC**G**CCC

2G-7: CCC**G**CCCCCCC**G**CCC

2G-8: CCC**G**CCCCCCCC**G**CC

2G-9: CC**G**CCCCCCCCC**G**CC

2G-11: C**G**CCCCCCCCCCC**G**C

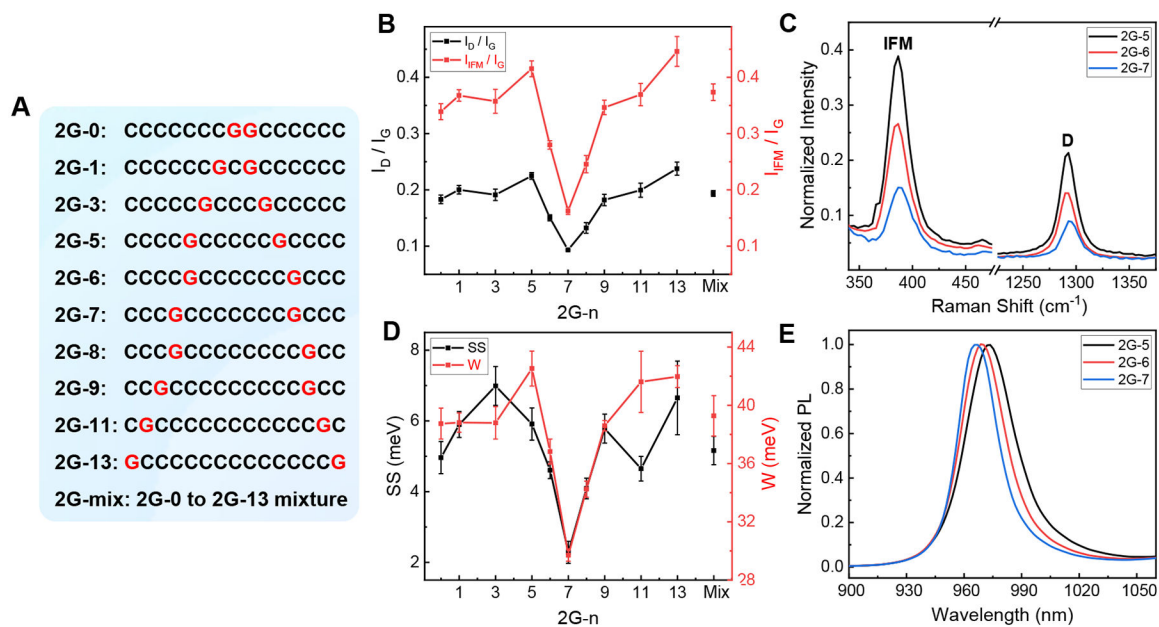2G-13: **G**CCCCCCCCCCCCC**G**

2G-mix: 2G-0 to 2G-13 mixture

Fig. 3. Screening DNA sequences for ordered defect array.
(**A**) DNA sequence used for the screening; (**B**) D and IFM peak intensity profile; (**C**) Raman spectra of 2G-5, 2G-6, and 2G-7 functionalized (8,3) (normalized by the "G" peak); (**D**) SS and W profile; (**E**) PL spectra of the three samples. Spectra in **C** and **E** are measured with 671 nm excitation. Also see Fig. S10 for original data.
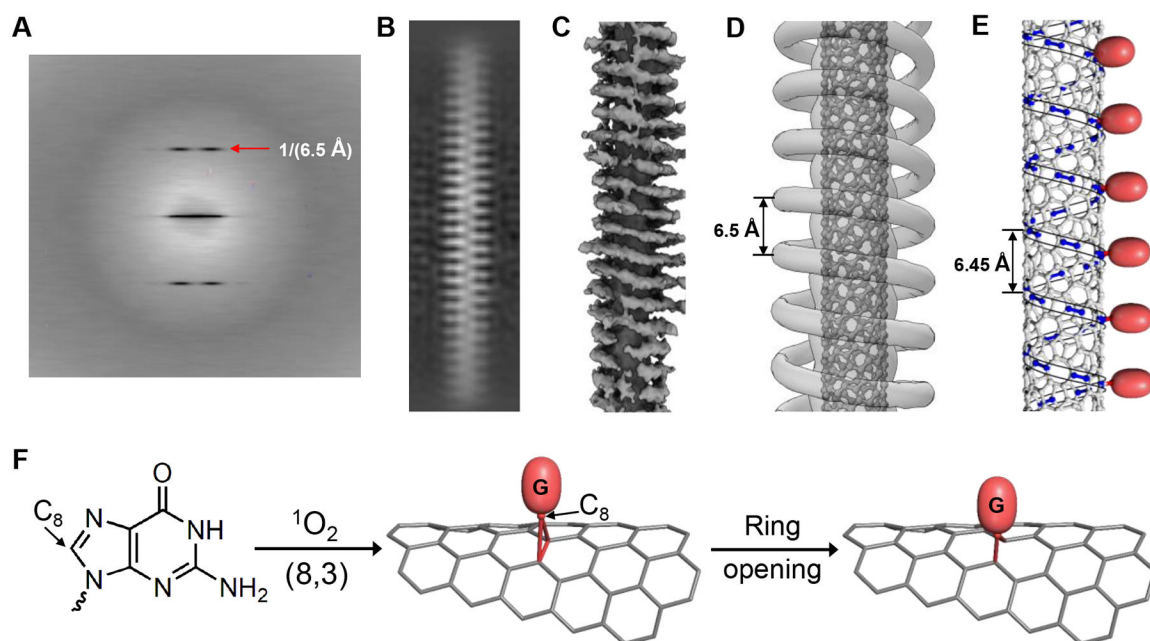
Fig. 4. Cryo-EM derived structure model for 2G-7 functionalized (8,3) and reaction mechanism.
(**A**) Averaged power spectrum from approximately 44000 particles. Red arrow points to a layer line with a spacing of $1/(6.5 \text{ Å})$ from the equator; (**B**) Image of 2D class average; (**C**) Low-resolution 3D map generated by unbiased, reference-free approach displays coherence that extends over an axial length of ≈ 10 nm; (**D**) 3D map corresponding to averaged density along the 6.5 Å pitch helix; (**E**) Carbon-carbon bonds that have maximum bond curvature, highlighted in blue along an armchair helical line of (8,3), along which every sixth carbon-carbon bond is modified by a guanine (red balls) according to modeling (Fig. S14A); (**F**) A proposed reaction mechanism.